GUIDED WAVE SCATTERING AT A DELAMINATION IN A QUASI-ISOTROPIC COMPOSITE LAMINATE: EXPERIMENT AND SIMULATION

F. Hervin* [a], L. Maio [b] and P. Fromme [a]

[a] Department of Mechanical Engineering, University College London, UK

[b] University of Naples "Federico II", Department of Industrial Engineering – Aerospace section, Naples, Italy

ABSTRACT

Carbon fibre composite laminates are increasingly being used for aerospace structures due to their low weight and improved mechanical performance. Impact damage can cause delaminations below the visible surface of the structure due to limited interlaminar strength. Guided ultrasonic waves can detect and characterize delaminations in composite laminates. The scattering of the A_0 Lamb wave mode at an artificial delamination, located at an asymmetric depth in a quasi-isotropic laminate, was investigated. Full field non-contact laser measurements were used to visualise wave trapping and scattered waves. A three-dimensional finite element model was developed and validated against the experiments. The influence of delamination shape and depth on guided wave scattering were studied. Small variations in delamination shape significantly affected the interference pattern on top of the delamination, but had limited effect on the scattered wave outside the delamination. Delamination depth was found to strongly influence the angular direction and amplitude of scattered waves. Implications for structural health monitoring were discussed.

Keywords: Composite laminate, Delamination, Scattering, Guided waves, CFRP, Lamb waves

INTRODUCTION

Fibre reinforced composite laminates are being increasingly used in a range of applications to reduce the weight of structures whilst improving their mechanical performance. However, composite laminates have limited interlaminar strength and are prone to low velocity impact damage [1]. Multilayer defects, consisting of delaminations (separation of the ply layers), fiber breakage and matrix cracking, occur throughout the thickness of the laminate, below the visible surface. The extent relates to the impact velocity and energy, the bending stiffness mismatch

* Corresponding author. flora.hervin.19@ucl.ac.uk

between adjacent ply layers due to different fibre orientations [2], as well as the thickness of the laminate [3, 4]**.** In thick laminates, impact damage has been demonstrated to propagate as a cone away from the impact location creating a 'pine tree' pattern [5]. In thin laminates, matrix cracking typically starts in the lowest ply layer due to bending stresses, and intra-ply cracks and interface delaminations propagate from the lowest surface up towards the impacted surface, resulting in a reverse pine-tree pattern [6]. A 'butterfly' pattern of (approximately) circular and ellipse shaped delaminations of varying size is often observed in the in-plane direction [7, 8, 9]. Whilst impact damage is complex and consists of multiple and interacting failure modes, delamination is considered the most dominant and critical failure mechanism in composites [10], and thus constitutes the focus of the present study. A relatively small impact load can cause extensive delamination damage below the laminate surface, resulting in barely visible impact damage (BVID) that is difficult to detect [11]. Subsequent application of external loads may induce fracture growth, leading to degradation of material properties (e.g., compressive strength reduction), and eventually catastrophic failure. Therefore, rapid and reliable non-destructive evaluation (NDE) techniques are required to locate and characterise delamination damage in multi-layered structures [12]. Radiographic [13, 14] and ultrasonic methods [15] are commonly used for composite components.

Guided ultrasonic waves can be exploited for rapid screening of large areas due to their long range propagation at low excitation frequencies, providing a promising in-situ structural health monitoring (SHM) solution for composites [16]. Generally, it is desirable to generate a single guided wave mode in a structure, below the cut-off frequency of the higher order wave modes. The fundamental symmetric S_0 mode has been used in several studies due to its low dispersion and high propagation velocity (first arrival) [17]. However, S_0 mode reflection is highly dependent on the through thickness location of the delamination, as no scattered wave is observed for disbonds at interfaces with zero shear stress [18]. On the other hand, the A_0 mode is sensitive to defects at any depth. It is more highly attenuated than the S_0 mode, resulting in shorter propagation distances. However, the A_0 mode has a slower phase velocity and shorter wavelength, and so has better resolution for small defects. The A_0 mode wave propagation shows less directional dependency compared to the S_0 mode for anisotropic composite structures [18].

Whilst numerical and experimental studies have demonstrated that guided waves can be used to detect delaminations, scattering at a delamination remains a complex problem. The anisotropy of a multi-layered plate influences the direction of scattered waves [19], [20]. Mode conversion and scattering occur when guided waves interact with a delamination. These effects can be used to detect and characterise damage [21]. Waves propagate in each of the sub-laminates above and below the delamination, typically with different velocities depending on the ply layup [22]. Numerous studies have reported that the amplitude of guided waves increased significantly over the delamination area, which could be exploited for damage detection [23, 24]. This effect is particularly pronounced for the A_0 mode, as the bending stiffness of thinner laminates is lower. The increase in amplitude is also caused by multiple reflections within the sub-laminates constructively interfering and generating standing waves, 'trapping' energy around the delamination area [25]. This increase in amplitude can be exploited for damage localization, and the difference in arrival times between multiple reflections can be used to estimate delamination size [26].

Wave trapping has been observed in both numerical simulations and laser doppler vibrometer measurements [27]. Several image processing techniques have been developed to take advantage of this behaviour and to highlight delaminations. Sohn et al. [25] proposed a standing wave filter in order to emphasise standing waves surrounding a delamination, whereas Testoni et al. [28] used a warped curvelet transform to remove the incident wave to isolate the reflected waves from the delamination. Kudela et al. [29] developed a selective weighted root mean square algorithm to generate clear damage maps for delaminations in cross ply panels with uniform thickness. The wave trapping phenomena has been used to distinguish between different sized delaminations at several depths for multilayer damage [30].

Scattered amplitudes and scattering directivity patterns depend on the ratio of delamination size to wavelength and the through thickness location of the defect [31]. Both back-scattered and forward scattered amplitudes can be observed, the amplitude of the latter being dependent on the phase difference between waves propagating in each of the sub-laminates [32]. When a delamination is located at an asymmetric depth, a high trapped amplitude can be observed on top of the thinner sub-laminate [23]. Delaminations located towards the mid-plane experience less wave trapping but have a higher scattered wave amplitude [33]. The scattering directivity pattern has been shown to be influenced by the fibre orientation of the outer plies of the laminate, due to fibre steering effects [22]. Scattering patterns depend on the layup sequence, even for laminates with the same number of ply layers [34]. Mei et al. found that the number of delaminations at the same location with different depths has an influence on the scattering pattern and the amplitude of trapped waves [35]. Mode velocity, wavelength, and deflection angle at a square delamination were found to vary with delamination depth [36].

Limited experimental studies have focused on guided wave scattering at a circular delamination. Murat et al. performed a systematic study on the influence of interlaminar damage depth and size through 3D Finite Element (FE) simulations with a zero volume square delamination, compared with experimental results for BVID [20]. Ng and Veidt [31] used 3D FE simulations to investigate the A_0 mode scattering at circular delaminations of various depths and sizes. The numerical model was verified experimentally for an artificial delamination created by an insert embedded at the laminate midplane. Pudipeddi et al. [37] performed a numerical investigation of mode conversion and scattering in a quasi-isotropic laminate containing circular delaminations of various depths and sizes. The discrete model was validated experimentally for the case of an undamaged laminate.

This contribution aims to improve the understanding of A_0 mode scattering at a circular delamination in a quasi-isotropic carbon fiber reinforced composite (CFRC) laminate. Full field, non-contact laser measurements were performed on a composite panel containing an artificial delamination located at an asymmetric depth, building on preliminary results [38]. A 3D FE model containing a zero-volume ellipse shaped delamination was developed to provide comparison to the experimental results and the convergence of the FE model was discussed. Two delamination shapes were modelled and compared with the experimental measurements. A systematic study was performed to investigate the influence of delamination depth on scattering.

EXPERIMENTAL MEASUREMENTS

Experiments were carried out on an 8-ply quasi-isotropic graphite/epoxy laminate with layup $[-45/45/90/0]_s$ and dimensions 600mm x 600mm x 1.6mm [39]. The panel was manufactured using unidirectional pre-preg plies and manual lay-up. The material properties of a single ply layer are given in Table 1. An artificial insert delamination was manufactured at the centre of the panel by inserting a circular polytetrafluoroethylene (PTFE) film, 15mm in diameter and 0.02mm thickness. The film was placed between the second and third plies during the layup process to give a delamination depth of 0.4mm. The resulting CFRC laminate was then cured in an autoclave. The cure cycle consisted of raising the temperature from 30°C to 175°C at 2.5 °C/min and was held at 175°C for 120 minutes at 3.5 atm. The position of the delamination was verified through an ultrasonic C-scan (Olympus OmniScan SX, 5 MHz phased array probe). An oval shaped crown was identified indicating detached plies, giving an actual flaw size of approximately 20 mm x 16 mm [40].

Table 1: Engineering constants for a single ply layer of the 8 ply CFRP composite plate, based on [30].

E_1 [GPa]	E_2 [GPa]	E_3 [GPa]	G_{12} [GPa]	G_{13} [GPa]	G_{23} [GPa]	ν_{12}	ν_{13}	ν_{23}	ρ [kg/m^3]
175	6.90	6.90	4.18	4.18	2.35	0.25	0.25	0.46	1520

A piezoelectric transducer (lead zirconate titanate (PZT) disk, PI Ceramic PIC-255, diameter 10 mm, thickness 0.25 mm) was bonded by cyanoacrylate glue to the surface of the composite plate 100 mm from the centre of the delamination location and was used to generate the A_0 guided wave mode. The excitation signal was a 5-cycle sine wave modulated by a Hanning window and was generated at 50kHz center frequency using a programmable function generator (Agilent 33220A). The excitation signal was amplified to 25V_{pp} (Krohn-Hite 7602M wideband amplifier) and applied to the transducer. A laser vibrometer (Polytec sensor head OFV-505, OFV-5000 vibrometer controller) attached to a scanning rig was used to measure the velocity of the out-of-plane displacement of the plate surface. The laser head was moved parallel to the sample both horizontally and vertically. Retroreflective tape was applied to the plate to improve the laser beam reflection and thus signal-to-noise ratio. The time signals were filtered using a band-pass filter with cut-off frequencies 25kHz above and below the centre frequency of excitation. The signals were then recorded and averaged 20 times using a digital storage oscilloscope before being saved to a PC to be further analysed in MATLAB R2019b.

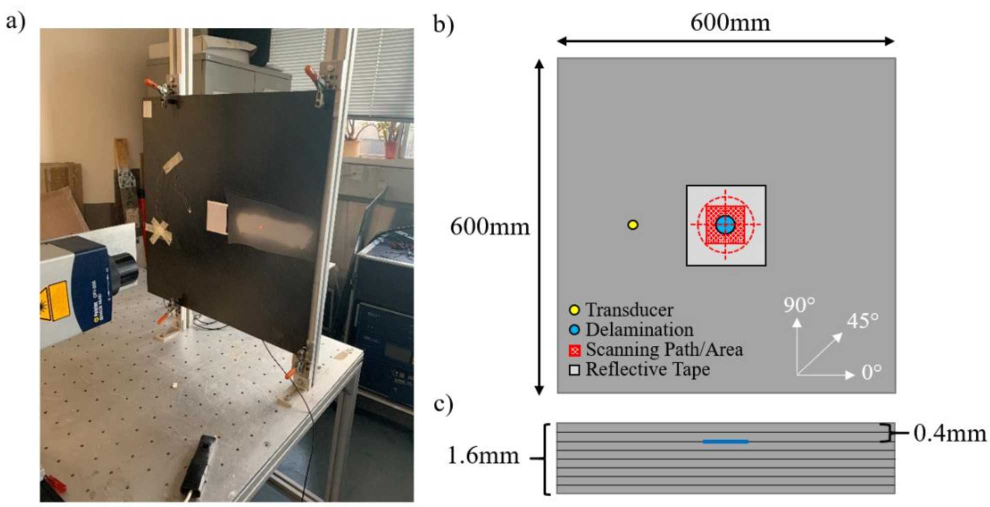

Figure 1: a) Experimental setup with laser head and composite plate specimen; b) schematic of quasi-isotropic composite laminate (top view) with transducer and damage locations marked. Red square indicates scanning area. Dotted lines indicate scanning paths across delamination; c) through thickness position of the delamination.

Three different scans were performed on the sample, as shown schematically in Fig. 1. A square area 40 mm x 40 mm centred on the delamination was scanned in 1 mm steps. A linear scan 70 mm in length was performed horizontally, and vertically, in 1 mm steps with each line crossing through the central point of the delamination. A circular scan centred on the delamination with radius 30 mm was performed in steps of 2°. To estimate the attenuation within the sample, additional line scans on an undamaged region of the plate were performed. The scans were performed along a 130mm line in 1mm steps along the 0° fibre direction. The first measurement point was at 10mm distance from the transducer. The reduction in amplitude along this line of points was used to estimate material damping.

FINITE ELEMENT MODEL

A full 3D layered FE model of a quasi-isotropic laminate with dimensions 600mm x 600mm x 1.6mm was developed. A model input file specifying the model geometry and parameters was generated in MATLAB and imported into ABAQUS/Explicit 2018 to perform the analysis. Eight node solid brick elements with reduced integration and hourglass control (C3D8R) were selected for the model. Each ply layer was modelled as a unidirectional layer of elements, with a single element through the thickness (0.2mm). The homogenous material properties given in Table 1 were assigned to each layer individually and the orientation of each layer was defined to produce the stacking sequence of the specimen ($[-45/45/0/90]_s$). A regular Cartesian mesh was used, as it has been shown to reduce numerical dispersion when modelling wave propagation [41].

A zero-volume delamination was incorporated into the model by overwriting existing elements at the delamination location, as shown schematically in Fig. 2. New nodes and elements, connected to one side of the plate, were defined over a square area with the approximate dimensions of the delamination. A node to node tie constraint was applied to form a circular shape (interpolated onto a Cartesian grid) as shown in Fig. 3. This procedure was also used to discretize an ellipse shaped delamination by defining a rectangular area of new nodes with dimensions of the major and minor axis of the ellipse. This approach provides an identical geometry to the more standard approach of two distinct regions with tie constraints [42], while allowing for straightforward automated generation of circular or ellipse shaped delaminations using the MATLAB code. For the present study, a 20mm x 20mm circular delamination was initially modelled and used as the standard case throughout.

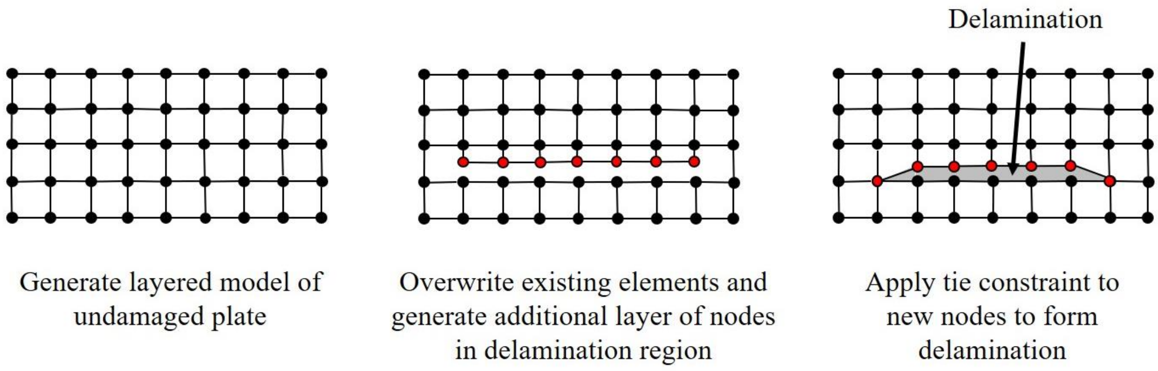

Figure 2: Schematic of procedure to model zero volume delamination. Through thickness view of mesh surrounding delamination region at different steps. Red nodes represent new nodes generated in the delamination area. Volume of delamination is exaggerated.

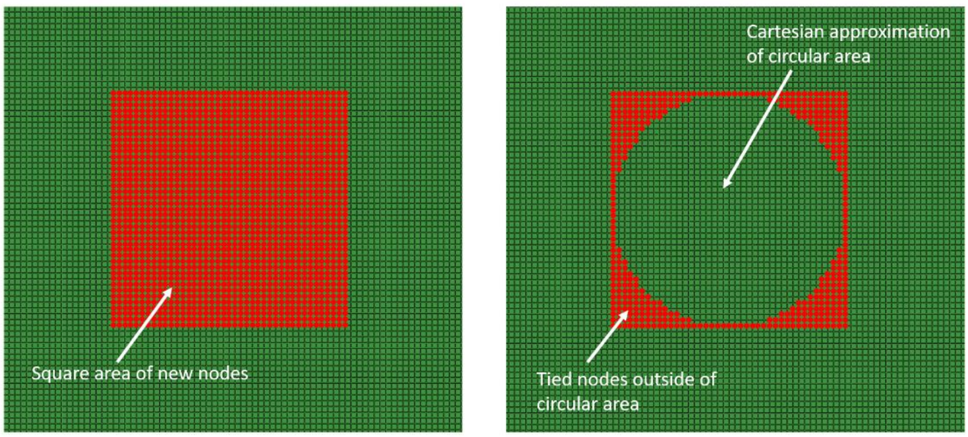

Figure 3: Close up top view of delamination region in ABAQUS: a) new nodes created in delamination region; b) tied nodes to form circular delamination area.

An out-of-plane force was applied to a single node located 100mm from the delamination centre to simulate generation of the A_0 mode. The excitation signal was a 5-cycle sine wave modulated by Hanning window with a centre frequency of 50kHz. Stiffness proportional damping was included into the model. The (Rayleigh) damping coefficient was set to β = 30ns. A 60mm x 60mm grid of monitoring points centred on the delamination was defined in 1mm steps. History output requests for the out-of-plane displacements were recorded at each measurement point. A 40mm x 40mm grid, bilinear interpolation onto a 30mm circle, and horizontal and vertical lines can be selected from this data during analysis for comparison to the experiments. A baseline model containing no damage was also created and the complex magnitude (amplitude and phase) of the incident wave at the center frequency (50 kHz) was calculated using Fast Fourier Transform (FFT). The magnitude of the scattered wave was isolated by subtracting the FFT baseline magnitude from the FFT magnitude of the signals for the simulations containing the delamination. Using the complex difference in the frequency domain retains both phase and amplitude information, removes the incident wave, and isolates the scattered component [43].

FE MODEL VALIDATION

MODEL CONVERGENCE

The element size was varied to determine the model convergence. An element size of 0.5mm x 0.5mm x 0.2mm was chosen initially. The thickness of the elements was kept constant at 0.2mm (one element per ply through the thickness), whilst the in-plane dimensions were varied to 0.4mm, 0.3mm, and 0.2mm respectively. The parameters for the convergence simulations are given in Table 2. The delamination was placed at 2 different depths: between the second and third plies (depth 0.4mm) to match the experimental specimen, and between the fourth and fifth plies (midplane of the plate, depth 0.8mm). A baseline simulation was run for each element size. The simulation time was 0.3ms for all element sizes. Additionally, monitoring points at each node along a 60mm horizontal line passing through the centre of the delamination were implemented.

The magnitude of the FFT at the centre frequency of the signal was extracted for each measurement point. Signals were time gated to remove any edge reflections. The magnitude was then normalised relative to the baseline magnitude of the FFT at the centre of the defect location (x = 0, y = 0). Figure 4 shows the full field of a 40mm x 40mm area centred on the delamination at depth 0.4mm for each element size. The incident wave propagates from left to right. Similar interference patterns were observed for each element size, but the amplitude of the guided wave field on top of the delamination showed some variation.

Table 2: Model parameters for convergence simulations.

Element size	Time increment (ns)	No. of elements (million)	Running time (hours)
0.5mm	50	12	4.5
0.4mm	25	18	9
0.3mm	25	32	15
0.2mm	20	32*	20

*0.2mm element size required plate size to be reduced to 400mm x 400mm x 1.6mm due to memory constraints.

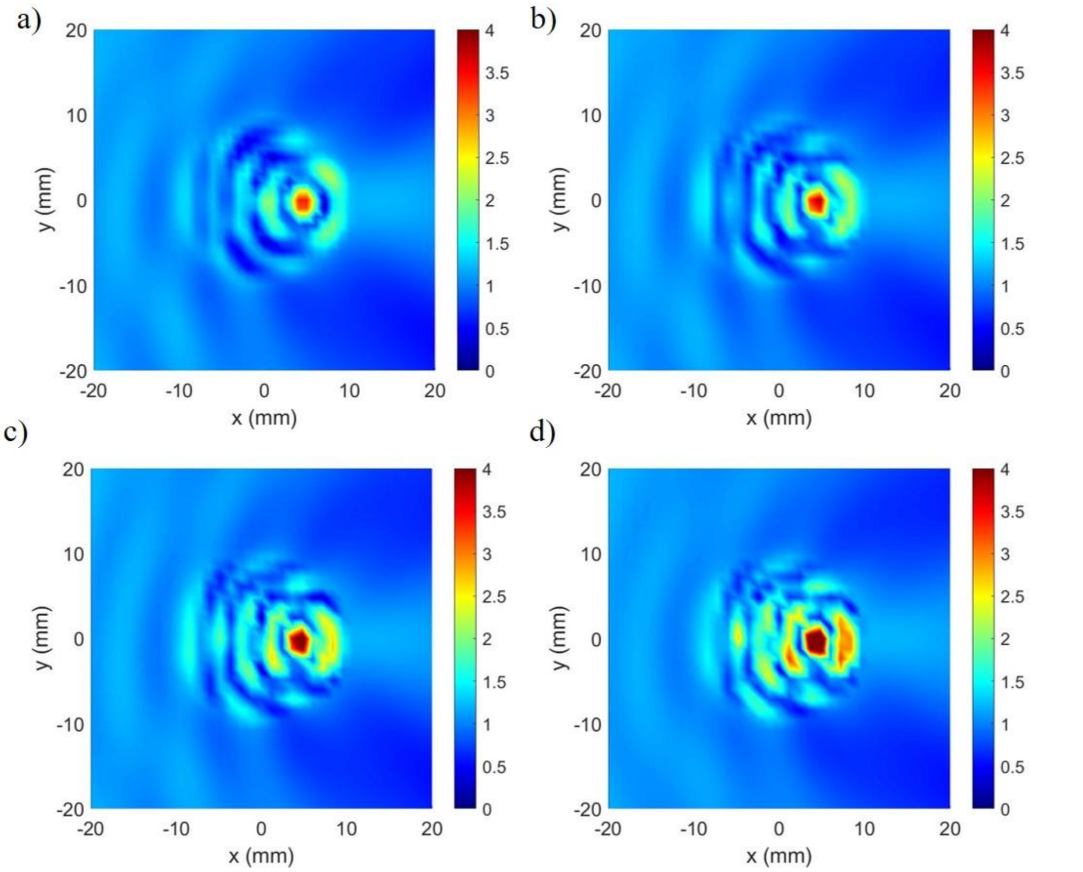

Figure 4: Magnitude of FFT at 50kHz for a 40mm x 40mm grid of measurement points centred on a 20mm x 20mm circular delamination; depth 0.4mm. In-plane element size: a) 0.5mm, b) 0.4mm, c) 0.3mm, d) 0.2mm.

The FFT magnitude at 50kHz along a horizontal line (y = 0) of measurement points for each element size is shown in Fig. 5. For a delamination located at the midplane of the plate (Fig. 5a, 0.8mm depth) the magnitude of the scattered wave is in good agreement to within 5% in front of, and inside, the delamination region for all element sizes. At delamination depth of 0.4mm (Fig. 5b) the magnitudes of the wavefield outside the delamination area are in agreement to within 6% for all element sizes. However, for the delamination region (x = -10mm to +10mm), whilst the overall scattering pattern and alignment of the peaks is similar between element sizes, the amplitudes of the individual peaks vary in magnitude by up to 45% as the element size is reduced, indicating that the model has not converged in this region. This is likely due to the waves propagating in the thin upper sub-laminate having a shorter wavelength (λ = 7mm) than those propagating through the full plate thickness (λ = 16mm), and so a smaller element size would be required to achieve full convergence on top of the delamination.

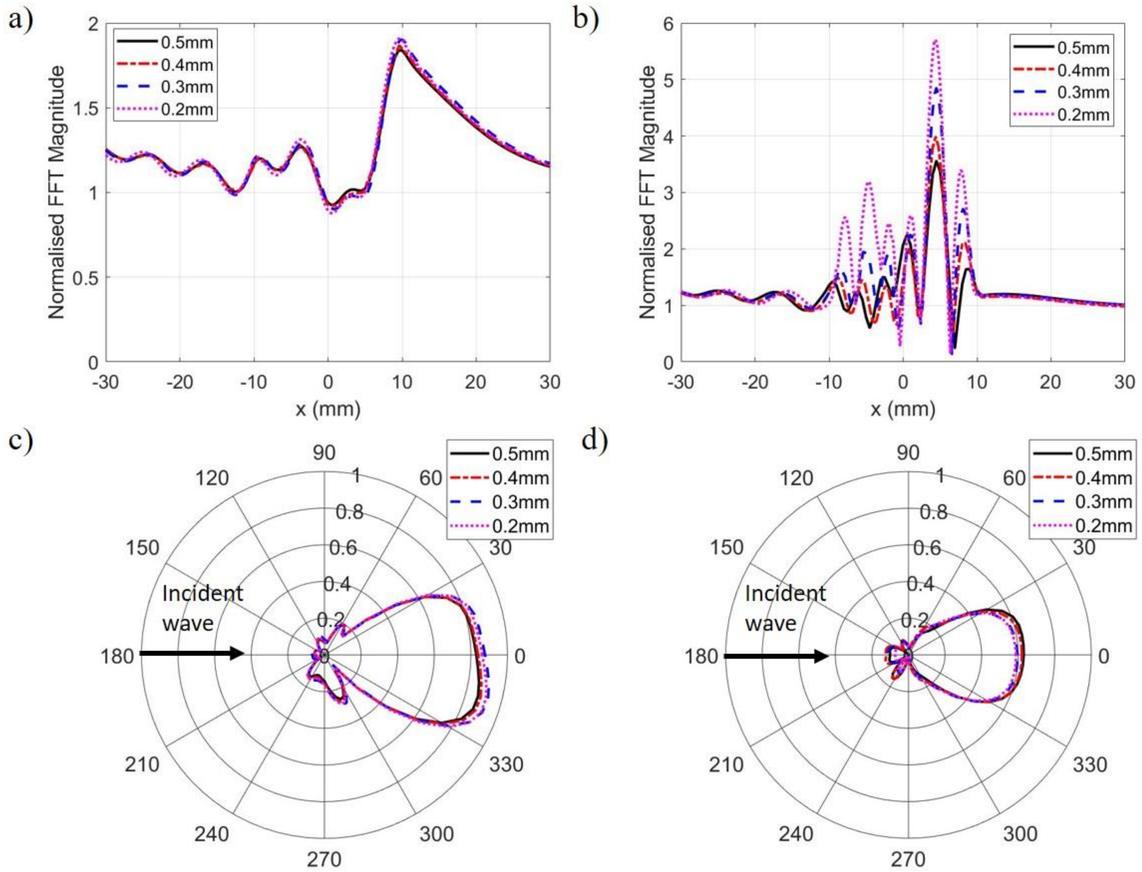

Figure 5: Normalised FFT magnitude (50 kHz) for different element sizes along a 60mm horizontal line of monitoring points for delamination depths a) 0.8mm, b) 0.4mm. Magnitude of baseline subtracted scattered wave for different element sizes for delamination depths c) 0.8mm, d) 0.4mm.

In addition to the interference pattern on top of the delamination, the scattered wave propagating in the undamaged region outside of the delamination area must be considered. Baseline subtraction was performed for a 30mm circle of measurement points in 2° increments. The 30mm radius is approximately twice the wavelength of the A_0 mode for the full plate thickness, sufficiently far from the defect to avoid the influence of near field scattering effects. Figure 5c/d show the angular magnitude of the scattered wave at delamination depths 0.8mm and 0.4mm respectively. At both delamination depths there is a large lobe around the 0° direction (+/-30°), indicating significant forward scattered amplitude. The amplitude is highest in the 0° direction and reduces towards the 30° direction, consistent with results in literature [20, 31, 37] The magnitudes are in agreement to within 5% for all element sizes at each depth, indicating that the model has converged in the undamaged region outside of the delamination.

Despite significant variation in peak magnitude, the qualitative features of the scattering on top (e.g., location of the peaks) of the delamination at 0.5mm element size reasonably match that of the smaller element sizes. In addition to the in-plane dimensions of the elements, the number of elements through the thickness per ply layer and the element type can also affect the numerical accuracy and hence the model convergence. It should be noted that employing a different element type, or two elements per ply layer, was found to affect the interference pattern on top of the delamination, but had limited effect on the scattered wave in the undamaged region of the laminate. In the context of SHM of composite structures, modelling the precise scattering behaviour on top of the delamination is of less interest as usually the aim of guided wave testing is to detect and quantify the scattered wave at some distance from the damage, so that damage can be localized. As the 0.5mm element size has been demonstrated to accurately model scattered wave propagation in the surrounding laminate whilst maintaining reasonable computation time, an element size of 0.5mm was selected for the further simulations presented in this study.

INFLUENCE OF DELAMINATION SHAPE

The ultrasonic C-scan results in [40] indicated that the artificial delamination has a slightly oval shape with a best estimate of 20mm length in the x-direction and 16mm width in the y-direction. The magnitude of the FFT at 50kHz over a 40mm x 40mm grid, horizontal line, and 30mm circle for an oval 20mm x 16mm shape and a circular 20mm x 20mm case were compared with the experimental measurements. Figure 6a shows the experimental FFT magnitude over a 40mm x 40mm grid of measurement points. The incident wave propagates from left to right. The magnitude significantly increases in a circular region with the approximate area of the delamination. The high magnitude over this region indicates that energy trapping is occurring within the delamination, which has been reported previously [20, 23, 25, 27]. The regions of high and low amplitude suggest that there are multiple reflections of guided wave modes within the delamination. A strong forward scattered wave can be observed at the right of the delamination, with two ‘shadow’ regions of low magnitude either side indicating destructive interference leading to lower wave amplitude. The small spots of high amplitude at the top of Fig. 6a are due to experimental noise.

An increase in FFT magnitude within the delamination region can be observed in both the 20mm x 16mm and 20mm x 20mm models (Fig 6b/c respectively). The delamination shape affects the shape of the high magnitude region. This could potentially be used to estimate delamination size from noncontact laser measurements. The predicted increase in magnitude relative to the surrounding regions is slightly lower for the numerical results than observed in the experiment. The forward scattered component can be observed in each of the simulations, but the drop in amplitude in the shadow regions either side of the forward lobe is lower than for the measurements. The scattering pattern on top of the 20mm x 16mm delamination matches the measured pattern more closely than the 20mm x 20mm circular defect, indicating that the delamination width affects the interference pattern on top of the defect. Whilst the scattering pattern on top of the delamination is sensitive to relatively small changes in delamination shape (mm), there is limited sensitivity to smaller geometric imperfections (e.g., sub-laminates not being perfectly flat, ply wrinkling). This is due to the wavelength of the A_0 mode being relatively large in comparison to these imperfections.

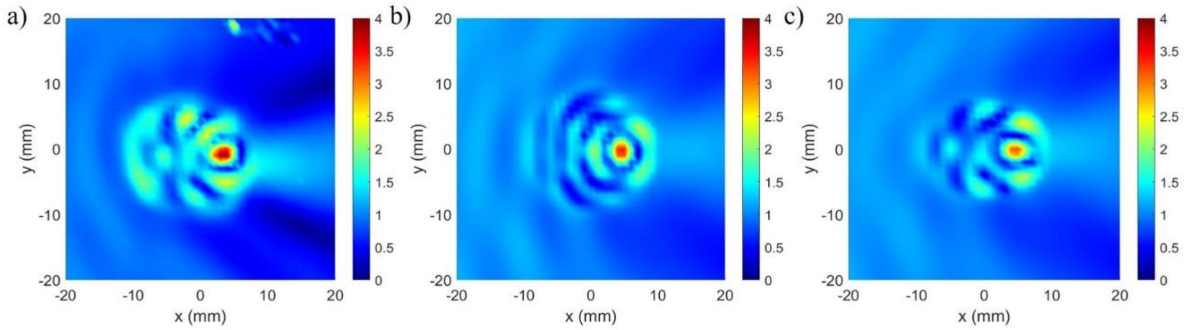

Figure 6: Normalised magnitude of FFT at 50kHz over a 40mm x 40mm grid of measurement points for a) experimental measurements; b) FEA 20mm x 16mm delamination; c) FEA 20mm x 20mm delamination.

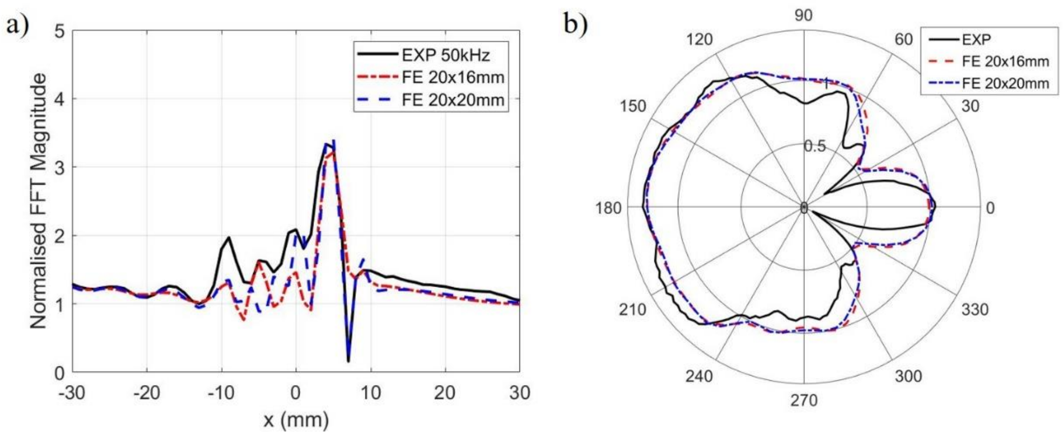

Figure 7: Measured and simulated magnitude of FFT at 50kHz for a) 60mm line of measurement points in 1mm steps, passing through the centre of the delamination; b) Circle of measurement points with radius 30mm (2° steps) centred on the delamination.

The measured FFT magnitude along a horizontal line of measurement points is denoted by the blue line in Fig. 7a. The magnitude decreases along the propagation direction until a sharp increase in magnitude is observed at the front edge of the delamination (x = -10 mm), consistent with the full field scan in Fig. 6a. The decrease in magnitude with propagation distance is expected due to wave spreading and attenuation. The variation in magnitude in front of the delamination occurs due to constructive and destructive interference with the backscattered wave. On top of the delamination, there are several amplitude peaks, with the highest peak at +4mm and a trough at +7mm. The forward scattered amplitude beyond 10mm is larger than that of the incident wave.

The wave amplitude for the FE simulation of the circular 20mm x 20mm delamination is denoted by the blue line in Fig. 7a. The incident wave, the peak at +4mm and trough at +7mm show good agreement with the measured values, to within 3%. However, the overall magnitude on top of the delamination and the forward scattered wave is lower than in the experiment. The incident wave for the 20mm x 16mm delamination model (red line Fig. 7a) has reasonable agreement within 9% of the measured values. The location of the major peak is in good agreement, however the trough at the edge of the delamination is not visible. Again, the magnitude on top of the delamination, and of the forward scattered wave, are lower than the measurements. In contrast to the 20mm x 20mm delamination, the location of the peaks within the delamination region of the 20mm x 16mm model match the experiment reasonably well. These results suggest that the interference pattern on top of the delamination is strongly influenced by the size and shape of the delamination, but that the forward and backward scattered waves are less sensitive to the exact defect shape.

The angular FFT amplitude of the scattered wave outside the damage area for the experiment (black), 20mm x 20mm delamination model (blue), and 20mm x 16mm delamination model (red) around a circle of measurement points with radius 30mm is shown in Fig. 7b. The measurements show a strong lobe in the 0° direction, consistent with the forward scattered wave observed in full field measurements in Fig. 6a. A steep drop in amplitude is observed at 30° and 330°, which corresponds to the location of the regions of destructive interference in the measured full wave field. The forward scattered amplitude is generally lower than the amplitude in the backscattered direction. The scattering pattern is reasonably symmetric.

The scattering patterns for the modelled delamination shapes agree with each other to within 3%, which suggests that delamination shape does not significantly influence the scattering pattern outside of the delamination. The magnitude of the scattered wave in the 0° and 180° directions agrees with the measurements to within 3% for the 20mm x 20mm delamination, and 5% for the 20mm x 16mm delamination. The forward scattered lobe is observed in the models, but the overall shape differs from the measurements. Two regions of lower amplitude are observed at 35° and 325° for both delamination sizes. However, the reduction in amplitude is not as strong as observed in the experiments, consistent with the full field results in Fig. 6. Overall, the FE results show good agreement with the experimental measurements, although certain features, such as the forward scattered lobe, were less distinct. It has been demonstrated that the interference pattern on top of the defect is strongly influenced by delamination shape and size, whereas the scattered wave around the delamination is similar for the considered cases.

INFLUENCE OF DELAMINATION DEPTH

The depth of a 20mm x 20mm circular delamination was systematically varied in 0.2mm increments (between each ply layer) and the scattering of the A_0 mode was simulated. The full field amplitudes over a 40mm x 40mm grid are shown for each delamination depth in Fig 8.

For a delamination at depth 0.2mm (Fig. 8a) a low amplitude region is observed over the delamination location, in contrast to most reports in literature [17]. A thin sub-laminate has a lower bending stress, so the amplitude of trapped waves on top of the delamination was expected to be high at 0.2mm delamination depth. At delamination depth 0.4mm (Fig. 8b), the amplitude of the scattering pattern on top of the delamination is higher, as observed previously and in line with literature. When the delamination is located at 0.6mm depth (Fig. 8c) some wave trapping on top of the delamination can be observed, although the scattering pattern is not as symmetrical as observed at 0.4mm depth. The forward scattered component can be observed between the 0° and +45° directions. The ply layup of the top sub-laminate at 0.6mm depth is asymmetric (-45°/+45°/90°) which could contribute to the steering of the forward scattered wave. At the midplane of the plate (0.8mm depth, Fig. 8d) almost no wave trapping on top of the delamination, but the highest 0° forward scattered component, are observed. A scattered component either side of the 0° wave can be observed (approximately +/-45° directions), although the amplitudes of the additional components are much lower. At the remaining delamination depths (Fig. 8e/f/g) only very limited wave trapping on top of the delamination is observed. This is likely due to the monitoring points being located on the opposite side of the plate to the thinner sub-laminate, where the higher amplitude reflections

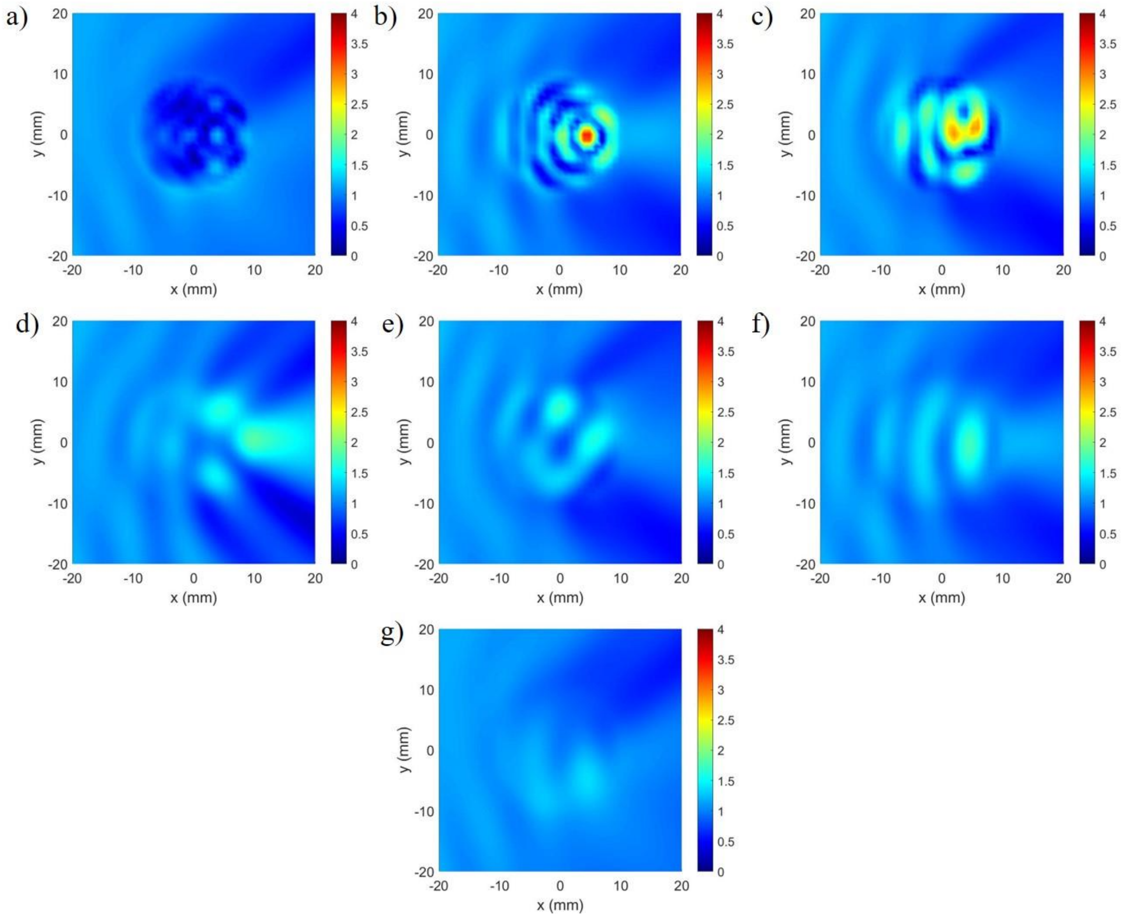

Figure 8: Normalised scattered wave amplitude (FFT at 50 kHz) for 20mm x 20mm circular delamination at range of delamination depths: a) 0.2mm; b) 0.4mm; c) 0.6mm; d) 0.8mm; e) 1.0 mm; f) 1.2mm; g) 1.4mm.

are observed. The amplitude outside of the delamination region at these depths indicate that the scattering outside of the delamination is similar at symmetric delamination depths.

In order to determine the influence of delamination depth on the scattering outside of the delamination, a baseline subtraction analysis was performed to determine the magnitude of the scattered wave on a 30mm circle centred on the delamination. Figure 9 compares the scattered wave for delaminations located at symmetric depths. Each pair of symmetric delamination depths has an identical scattered wave pattern outside the delamination area. Fig. 9a shows a narrow lobe (approximately 0.4 of the amplitude of incident wave) directed towards the 330° direction for delamination depths 0.2mm and 1.4mm, likely due to energy focusing along the fibres of the outer -45° direction plies. At delamination depths 0.4mm and 1.2mm (Fig. 9b) a symmetric lobe in the 0° direction is observed, with a higher amplitude than the 0.2mm and 0.6mm cases, which could be due to the symmetric layup of the top sub-laminate (+/-45° direction). Increasing the delamination depth to 0.6mm or 1.0mm generates a lobe with the highest amplitude in the 30° direction. The highest amplitude of the scattered wave occurs for

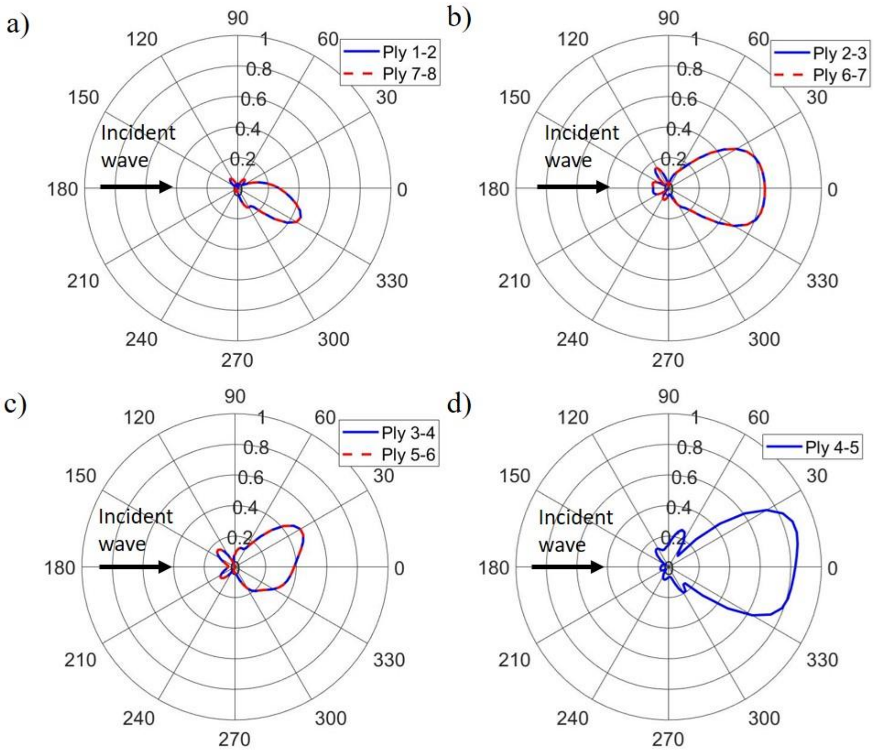

Figure 9: Scattered wave around a 30mm circle of measurement points, obtained via baseline subtraction. Symmetric delamination depths plotted together: a) ply 1-2 (0.2mm) and ply 7-8 (1.4mm) b) ply 2-3 (0.4mm) and ply 6-7 (1.2mm) c) ply 3-4 (0.6mm) and ply 5-6 (1.0mm) d) ply 4-5 (0.8mm – midplane).

a delamination at the midplane of the plate (Fig. 9d). Constructive interference due to the symmetric sub-laminae could contribute to the higher amplitude.

The results presented in Fig. 9 indicate that the delamination depth and ply lay-up of the sub-lamina influence the direction of scattered waves outside of the delamination. The scattered wave can therefore be used to determine two possible through thickness locations of the delamination. At all delamination depths the backscattered amplitude is small, which suggests that a pulse-echo detection approach for SHM of the composite plate would have limited sensitivity. For a pitch-catch approach, the forward scattered wave shows a counterintuitive increase in amplitude behind the delamination rather than the often expected decreased amplitude behind the damage. The pitch-catch approach could be more reliable for detecting delaminations, but care must be taken, as the direction of the forward scattered lobe may differ from the incident propagation direction.

This investigation has focused on guided wave interaction with simple circular and ellipse shaped delaminations. Whilst these damage shapes can occur as part of multilayer damage, wave scattering around real BVID will likely differ from that of the idealised shapes presented here. The procedure for incorporating damage into the FE model presented in this work could potentially be extended to incorporate more complex damage if separate damage data is available, for example X-ray CT data [7]. Some studies have focused on detection and sizing of the major (largest) delamination at real BVID [44] and wave trapping has been demonstrated to be sensitive to multi-layered delaminations [30]. This indicates that the methodology presented in this work could be applied to more realistic damage types.

CONCLUSIONS

Guided wave propagation and scattering at an ellipse shaped delamination in a quasi-isotropic composite laminate has been investigated through experiments and FE simulation. The artificial delamination was located asymmetrically through the full thickness of the plate. Full field non-contact laser measurements verified the wave trapping phenomena with increased amplitude on top of the delamination, and visualised the forward scattered wave and shadow regions behind the defect. A full 3D layered FE model containing a zero-volume delamination was developed and showed good agreement with the experimental results. The convergence of the model was investigated by varying element size and good convergence was observed in the undamaged laminate outside of the delamination region. Inside the delamination significant amplitude variation was observed between element sizes, however the qualitative location of the peaks showed good agreement. The influence of delamination shape and depth were investigated numerically. Small changes in delamination shape were found to have a significant effect on the interference pattern on top of the delamination, but limited effect on the scattered wave directivity some distance from the defect. The region of high amplitude on top of the delamination could be used to estimate delamination size and shape. Delamination depth significantly influenced both the interference pattern on top of the delamination, and the scattering pattern outside of the delamination, due to the different ply layups of the sub-laminate. Generally, both wave trapping and forward scattered components were observed for delaminations located between the outer plies of the laminate. The largest forward scattered amplitude occurred at the mid-plane delamination, likely due to the symmetrical layup of the sub-laminates. The incident wave was removed, and the scattered wave was isolated by performing a complex difference baseline subtraction to obtain the angular energy distribution. At all delamination depths negligible backscattered amplitude was observed, indicating that delaminations may be difficult to detect using a pulse-echo SHM approach. The strong forward scattered amplitude indicates that a pitch-catch approach could be more appropriate, although care must be taken as the forward scattered component is not always directed along the incident wave propagation direction. The delamination shapes investigated in this study are idealised compared to real BVID, however the methodology presented could be extended to incorporate more complex damage types.

DATA AVAILABILITY

The raw and processed data required to reproduce these findings cannot be shared at this time as the data also forms part of an ongoing study.

REFERENCES

[1] Cantwell W and Morton J. Geometrical Effects in the Low Velocity Impact Response of CFRP. *Compos Struct* 1989; 12:39–59.

[2] Choi Y and Chang FK. A Model for Predicting Damage in Graphite/Epoxy Laminated Composites Resulting from Low-Velocity Point Impact, *J Compos Mater* 1992; 26(14):2134–2169.

[3] Hayat K and Ha SK. Low-velocity impact-induced delamination detection by use of the S0 guided wave mode in cross-ply composite plates: A numerical study. *J Mech Sci Technol* 2014; 28(2):445–455.

[4] Shyr TW and Pan YH. Impact resistance and damage characteristics of composite laminates. *Compos Struct* 2003; 62:193–203.

[5] Cantwell W and Morton J. Detection of impact damage in CFRP laminates. *Compos Struct* 1985; 3:241–257.

[6] Abrate S. *Impact on composite structures.* Cambridge: Cambridge University Press 1998

[7] Leckey C, Rogge M and Parker F. Guided waves in anisotropic and quasi isotropic aerospace composites: Three-dimensional simulation and experiment. *Ultrasonics* 2014; 54:385–394.

[8] Wertz J, Wallentime S, Welter J, et al. Volumetric characterization of delamination fields via angle longitudinal wave ultrasound. *AIP Conf Proc* 2017; 1806:090006.

[9] Mesnil O, Leckey CAC and Ruzzene M. Instantaneous and local wavenumber estimations for damage quantification in composites. *Struct Heal Monit* 2015; 14(3):193–204.

[10] Wisnom MR. The role of delamination in failure of fibre-reinforced composites. *Philos Trans R Soc A Math Phys Eng Sci* 2012; 370:1850–1870.

[11] Prichard JC and Hogg PJ. The role of impact damage in post-impact compression testing. *Composites* 1990; 21(6):503–311.

[12] Ibrahim ME. Nondestructive evaluation of thick-section composites and sandwich structures: A review. *Compos Part A Appl Sci Manuf* 2014; 64:36–48.

[13] Bull DJ, Spearing SM, Sinclair I, et al. Three-dimensional assessment of low velocity impact damage in particle toughened composite laminates using micro-focus X-ray

computed tomography and synchrotron radiation laminography. *Compos Part A Appl Sci Manuf* 2013; 52:62–69.

[14] Shoukroun D, Massimi L, Endrizzi M, et al. Enhanced composite plate impact damage detection and characterisation using X-Ray refraction and scattering contrast combined with ultrasonic imaging. *Compos Part B Eng* 2020; 181:107579.

[15] Smith RA, Nelson LJ, Xie N, et al. Progress in 3D characterisation and modelling of monolithic carbon-fibre composites. *Insight Non-Destructive Test Cond Monit* 2015; 57(3):131–139.

[16] Hall JS, Fromme P and Michaels JE. Guided wave damage characterization via minimum variance imaging with a distributed array of ultrasonic sensors. *J Nondestruct Eval* 2014; 33(3):299–308.

[17] Tan KS, Guo N, Wang BS, et al. Experimental evaluation of delaminations in composite plates by the use of lamb waves. *Compos Sci Technol* 1995; 53:71–84.

[18] Guo N and Cawley P. The interaction of Lamb waves with delaminations in composite laminates. *J Acoust Soc Am* 1993; 94(4):2240–2246.

[19] Chiu WK, Rose LRF and Nadarajah N. Scattering of the Fundamental Anti-symmetric Lamb Wave by a Mid-plane Edge Delamination in a Fiber-composite Laminate. *Procedia Engineering* 2017; 188:317–324.

[20] Murat B, Khalili P and Fromme P. Scattering of guided waves at delaminations in composite plates. *J Acoust So Am* 2016;139(6):3044–3052.

[21] Toyama N and Takatsubo J. Lamb wave method for quick inspection of impact-induced delamination in composite laminates. *Compos Sci Technol* 2004; 64(9):1293–1300.

[22] Feng B, Ribeiro AL, and Ramos HG. Using guided ultrasonic wave inspection to quantify the length of delaminations in composite laminates. *AIP Conf Proc* 2018; 1949:230027.

[23] Ramadas C, Balasubramaniam K, Joshi M, et al. Interaction of guided Lamb waves with an asymmetrically located delamination in a laminated composite plate. *Smart Mate Struct* 2010; 19(6):065009.

[24] Hayashi T and Kawashima K. Multiple reflections of Lamb waves at a delamination. *Ultrasonics* 2002; 40:193–197.

[25] Sohn H, Dutta D, Yang JY, et al. Delamination detection in composites through guided wave field image processing. *Compos Sci Technol* 2011; 71(9):1250–1256.

[26] Toyama N, Noda J, and Okabe T. Quantitative damage detection in cross-ply laminates using Lamb wave method. *Compos Sci Technol* 2003; 63:1473–1479.

[27] Tian Z, Yu L, and Leckey C. Delamination detection and quantification on laminated composite structures with Lamb waves and wavenumber analysis. *J Intell Mater Syst Struct* 2015; 26(13):1723–1738.

[28] Testoni N, De Marchi L and Marzani A. Detection and characterization of delaminations in composite plates via air-coupled probes and warped-domain filtering. *Compos Struct* 2016; 153:773–781.

[29] Kudela K, Wandowski T, Malinowski P, et al. Application of scanning laser Doppler vibrometry for delamination detection in composite structures. *Op Lasers Eng* 2017; 99:46–57.

[30] Leckey C and Seebo J. Guided wave energy trapping to detect hidden multilayer delamination damage. *AIP Conf Proc* 2015; 1650:1162.

[31] Ng CT and Veidt M. Scattering analysis of fundamental anti-symmetric lamb wave at delaminations in composite laminates. *J Acoust Soc Am* 2011; 129(3):1288–1296.

[32] Samaitis V, Mažeika L and Rekuviene R. Assessment of the length and depth of delamination-type defects using ultrasonic guided waves. *Appl Sci* 2020; 10(15):5236.

[33] Gupta S and Rajagopal P. Effect of ply orientation and through-thickness position of delamination on the reflection of fundamental symmetric S0 Lamb mode in GFRP composite plate structures. *Ultrasonics* 2018; 90:109–119.

[34] Mei H and Giurgiutiu V. Characterization of multilayer delaminations in composites using wavenumber analysis: numerical and experimental studies. *Struct Heal Monit* 2021; 20(3):1004–1029.

[35] Migot A, Mei H and Giurgiutiu V. Numerical and experimental investigation of delaminations in a unidirectional composite plate using NDT and SHM techniques. *J Intell Mater Syst Struct*, 2020.

[36] Panda R, Rajagopal P and Balasubramaniam K. Characterization of delamination-type damages in composite laminates using guided wave visualisation and air-coupled ultrasound. *Struct Heal Monit* 2017; 16(2):142–152.

[37] Pudipeddi GT, Ng C, and Kotousov A. Mode Conversion and Scattering of Lamb Waves at Delaminations in Composite Laminates. *J Aerosp Eng* 2019; 32(5):04019067.

[38] Maio L, Hervin F, and Fromme P. Guided wave scattering analysis around a circular delamination in a quasi-isotropic fiber-composite laminate. *Proc SPIE* 2020; 11381:113810Q.

[39] Maio L, Ricci F, Memmolo V, et al. Application of laser Doppler vibrometry for ultrasonic velocity assessment in a composite panel with defect. *Compos Struct 2018;* 184:1030–1039.

[40] Maio L, Memmolo V, Boccardi S, et al. Ultrasonic and IR Thermographic Detection of a Defect in a Multilayered Composite Plate. *Proc Eng* 2016; 167:71–79.

[41] Celep Z and Bažant ZP. Spurious reflection of elastic waves due to gradually changing finite element size. *Int J Numer Meth Eng* 1983; 19:631–646.

[42] Köllner A. Predicting buckling-driven delamination propagation in composite laminates: An analytical modelling approach. *Compos Struct* 2021; 266:113776.

[43] Fromme P. Guided wave sensitivity prediction for part and through thickness crack-like defects. *Struct Heal Monit* 2020; 19(3):953–963.

[44] Toyama N and Takatsubo J. Lamb wave method for quick inspection of impact-induced delamination in composite lamintes. *Compos Sci Technol* 2004; 64(9):1293–1300.